RESEARCH ARTICLE

Thermal and Chemical Dynamics in Magnetohydrodynamic Williamson Fluid Flow over a Stretching Cylinder under Heat/Mass Flux Effects Using Optimal Homotopy Analysis Method

Nimra Riaz[1] **and Muhammad Sohail**[1,*]

[1] Institute of Mathematics, Khwaja Fareed University of Engineering & Information Technology, Rahim Yar Khan 64200, Pakistan

Abstract

The knowledge on understanding non-Newtonian fluid dynamics influences and behaviors in magnetic and nanoscale effects of transport is also important to the advanced processes of engineering. The current paper examines MHD flow and heat transfer of a Williamson nanofluid across a stretching cylindrical surface, taking into consideration Hall current and chemical reaction and non-Fourier heat and mass flux that is described by the Cattaneo Christov theory. The transport of Nanoparticles is explained in terms of Buongiorno model of thermophoresis and Brownian movement. Similarity variables are used to transform the governing nonlinear equations and then analytically solved via Optimal Homotopy Analysis Method. The parametric study of parameters like $M = 0.5 - 2.0$, $\gamma = 0.1 - 5.0$, $Nt = 0.1 - 0.5$, $Nb = 0.1 - 0.3$, $\delta t = \delta c = 0.1 - 0.5$, and $Kr = 0.1 - 1.0$ indicates that the values of the magnetic field, relaxation times, Hall currents, and diffusion of nanoparticles have a considerable effect on the flow, thermal, and concentration fields. The results have interesting applications in polymer extrusion, thermal control of nano-devices, magnetic drug delivery, and manufacturing smart materials.

Keywords: williamson fluid, Magnetohydrodynamics (MHD), hall effect, buongiorno model, cattaneo-christov flux, chemical reaction, nanofluid, stretched cylinder, optimal homotopy analysis method.

1 Introduction

The study industrial thermal impacts and chemical transformations in nanofluid fluxes has grown in importance in the past few years, owing to their practical significance in a wide range of technical and biological industries. Dissipation, or the conversion of energy from motion into the heat inside liquids that are viscous, is critical in optimizing power systems

Submitted: 19 July 2025
Accepted: 30 August 2025
Published: 22 November 2025

Vol. 1, **No.** 2, 2025.
10.62762/IJTSSE.2025.383195

***Corresponding author:**
✉ Muhammad Sohail
muhammad.sohail@kfueit.edu.pk

Citation
Riaz, N., & Sohail, M. (2025). Thermal and Chemical Dynamics in Magnetohydrodynamic Williamson Fluid Flow over a Stretching Cylinder under Heat/Mass Flux Effects Using Optimal Homotopy Analysis Method. *International Journal of Thermo-Fluid Systems and Sustainable Energy*, 1(2), 46–63.

such as solar collectors, thermodynamic storage tanks, and maintenance technologies since it affects thermal efficiency and lowers wear. Meanwhile, chemical reactions in conjunction with fluid flow are critical to processes such as wastewater treatment, chemical manufacture, polymer synthesis, and targeted medication delivery, where regulating reaction kinetics improves performance and product quality. Learning these effects in complex fluids like Williamson nanofluids under magnetic and thermal influences is very essential in enhancing the present cooling mechanisms, biomedical applications, and processing. A significant role of magnetohydrodynamic (MHD) fluid flow involving the interaction of electrically conducting fluid with magnetic field is a subject of research, and its numerous applications in engineering sector especially in cooling systems study, dynamics of plasma and generation processes of energy Das et al. [1]. Non-Newtonian fluids—such as the Williamson fluid—offer significant advantages for analyzing the often intricate flow behaviors encountered in biological, industrial, and material-processing systems, as noted by Böhme [2]. Shear-thinning or shear- thickening characterizes these fluids and thus they better reflect real world applications than the conventional Newtonian fluids. To include the effect of viscous dissipation and also the Joule heating, Makkar et al. [3] studied the effect of magnetohydrodynamics (MHD) on bio convection nanofluid flow. The case of Turkyilmazoglu et al. [4] to investigate analyses flow and heat transfer in concentric annuli with an inner annulus moving in a shrinking mode and an outer annulus stationary. It offers an insight into the development of a boundary layer and thermal behavior of confined geometries with constricting boundary. Hamid et al. [5] studied the behavior of diffusion of nanoparticle in Williamson nanofluid flow in MHD and they also investigate that whether multiple solutions are present or not besides the presence of slip mechanism at the boundary and impact of slip and magnetic effects on both the flow characteristic and thermal behavior. Harfouf et al. [6] examined the literature of magnetohydrodynamic (MHD) flow Williamson fluid (and considering the effects of thermal radiation and Ohmic heating) on an inclined channel. Khan et al. [7] examined the bioconvective flow of a nanofluid micropolar fluid over a vibrating porous surface taking into consideration a non-linear thermal radiation, viscous-dissipation, and suction. It examines the impact of these on the fluid flow, heat transfer, and dynamics of particles in the biomedical practice. Ramzan et al. [8] to study Free convection flows in saturated porous media with time-varying surface heat flux with the flow being solved exactly finding several solutions analytically. The findings indicate non-uniqueness in the thermal behavior indicating that there is the potential of bifurcation in the heat flow case. Nadeem et al. [9] examined entropy generation, as well as irreversibility, in MHD channel flow of Williamson fluid, where combined convective-radiative boundary conditions were used. The test applies an insight into the entropy generation through magnetic fields, thermal radiation, and convective heat exchange and thus gives an idea of the efficiency and irreversibility of the flow system. Ahmad et al. [10] examined the transport of thermal and solutal energy and the generation of entropy in the rectilinear flow of hybrid nanofluid of a vertically rotating cylinder. Turkyilmazoglu [11] to investigate provides the direct solutions of the momentum and the thermal boundary layers formed through a long circular cylinder in a still fluid. It is analytically insight into the coupling between viscous and thermal effects of diffusion around cylindrical bodies.

At practical applications the flow of such fluids is generally in the presence of the electromagnetic fields and here the MHD, effect, over which Hall current has significant effect on the fluids dynamics and the heat transfer processes Shah et al. [12]. Pivotal in changing the velocity profiles and temperature distributions are the Hall currents that are produced by the magnetic field, interacting with charged particles within the fluid, essentiality in systems when electrically conductive fluids are considered such as plasmas or nanofluids. More so, the comparison of heat and mass transfer in these systems has been greatly enhanced through generalised flux terms. Turkyilmazoglu [13] The investigated study of nonlinear similarity solutions of flows due to stretching or moving sheets applies to the case of manual atomization and the process of electrospinning. It illustrates the impact of the air resistance on the flow dynamic, and it provides ideas on dynamics of fluid stretching in industries. The latter ones, including a heat and mass flux law proposed by Cattaneo and Christov, permit the more precise description of the energy and particles moment transfer processes, especially in a non-instantaneous regime Cattaneo [14] and Ván [15]. Generalized models are necessary in describing the delayed reaction of temperature and concentration gradients in fluids, particularly, when there is presence of nanoparticles and chemical

reactions. Ali et al. [16] studied the MHD flow of hybrid nanofluid over an extended cylinder with the following considerations, Cattaneo Christov heat flux model and radiation effects. Khan et al. [17] computed, using generalized Fourier and Fick laws, movement of the two dimensional Carreau fluid under normal surface condition. A numerical calculation on heat and mass transport in Williamson material with modified flux models is investigated by Sohail et al. [18] and the solutions are performed by employing an optimal homotopy analysis method (OHAM) where the influence of modified heat and mass fluxes, together with non-Newtonian fluid behavior on the temperature and concentration. Nadeem et al. [19] investigated the flow of fluid that was viscoelastic along with heat flux model powered by the Cattaneo-Christov theory and Newtonian heating. To investigate the implication of Hall current, magnetic field, geometry of a channel of the Hall current they are proposed by Li et al. [20] to study the effects. Shafiq et al. [21] study investigates how the interplay of thermal and solutal stratification, along with radiative heat transfer, influences the flow dynamics, temperature distribution, and mass transfer in the system. Khan et al. [22] study analyzes how the inclusion of this non-Fourier heat conduction model influences temperature distribution, velocity profiles, and heat transfer efficiency in the fluid system.

This research endeavors to apply Buongiorno model to a Williamson fluid flow when MHD is accounted and how convective boundary conditions together with chemical reactions can be taken into account is pursued. The fluid system also has chemical reactions that complicate the transport processes. Chemical species may interact in the flow and change the concentration profiles affecting the general thermal behavior. It has been depicted through studies that homogenous and heterogeneous chemical processes may bring massive transformation in flow and heat transfer behaviors Ali et al. [23]. Khan et al. [24] covered the impacts of Brownian motion and thermophoresis on MHD mixed pertinent convective flow of a second grade nanofluid over a stretching sheet including the hall effect. Sohail et al. [25] examine mass and heat transfer nature of non-Newtonian flow that is characteristic to the Williamson nanofluid over a stretched sheet by considering such effects as chemical reactions, viscous dissipation, magnetic field and slip velocity. In one type of non-Newtonian model a study of thermal transportation in a ternary hybrid nanofluid flow was investigated by taking into account homogenous and heterogenous chemical reactions by a vertical cylinder by Hussain et al. [26]. In this work Abbas et al. [27] Investigates the viscous flow of a pipe with a porous wall situated in the magnetic fields, the asymptotic magnetohydrodynamic effect is studied. It provides analytical feedback to flow alteration because of wall suction/injection and electromagnetic interactions. Zaman et al. [28] considered the Williamson MHD nanofluid flow over a slender cylinder, in the consideration of the effects of radiation. The experiment investigates the effects of magnetic fields and heat radiations on the flow behavior, heat transfer, and distribution of nanoparticle within the system which can offer information relating to enhancement of thermal management systems. Rauf et al. [29] explores Hall current and morphological effects of MHD micropolar non-Newtonian tri-hybrid nanofluid in between two parallel surfaces. Rasheed et al. [30] discusses the unsteady magnetohydrodynamic (MHD) motion of Casson nanofluid supra a vertical cylinder together with the effects of Brownian movement and viscous dissipation.

Even despite many studies on non-Newtonian fluid dynamics subjected to magnetic fields such as Williamson fluid dynamics and magnetic fluid forces, several of them have been on planes, and classical Fourier and Fick laws of heat and mass transport. The applicability of Cattaneo-Christov models, that include effects of temperature relaxation and solutal relaxation, in order to overcome the drawback of limitless propagation speed of classical models, have hardly been explored in this form. In addition, current literature fails to examine the combined effects of Hall currents, kinetics of chemical reactions and stretched cylindrical flows which are critical in a precise modeling of high temperature and or rotating and electrically conducting fluids in the industrial and geophysical environment. The current paper is an attempt to fill this gap by examining the MHD flow of a Williamson fluid over a radially stretched cylinder in the presence of Hall effects as well as Cattaneo-Christov heat and mass fluxes, and chemical reactions. This rigorous formulation, to our knowledge is a new contribution that entails a combination of many complex physical phenomena within the same coherent model giving a better understanding of nonlinear behavior of viscoelastic MHD flows with plausible thermal and mass diffusion properties.

2 Mathematical formulation

Mathematically, the MHD Williamson fluid flow over an extended cylinder can be modeled with the help of Hall current, thermodynamics, chemistry, and mass and heat flux Cattaneo-Christov models using cylindrical coordinate (r, θ, z). Perhaps, the 2-dimensional laminar flow of nanoliquid with the steady and incompressible flow against stretched porous cylinders. The axial direction radius a is toward the axial direction. Further, $z - axis$ is parallel and $r - axis$ perpendicular to the cylinder respectively. The grid of coordinates is in Figure 1. Additionally, $U_w(z) = \frac{U_o}{l}$, C_w and T_w stand for the surface velocity of a stretchy cylinder, surface thermal, and surface solutal, respectively.

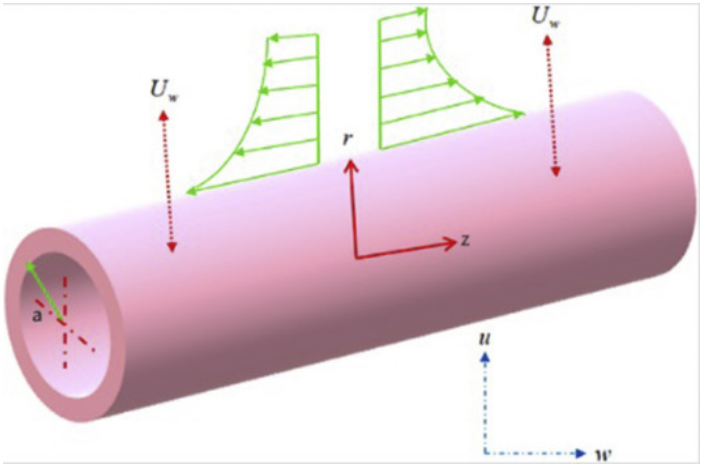

Figure 1. Geometry problem.

In this T_∞ and C_∞ indicate the general temperature and quantity, correspondingly. Here a radial magnetic field of the intensity $\frac{B_0 R}{r}$ is applied to the radial direction. In this mathematical description, $(\frac{B_0 R}{r}, 0, 0)$ is the magnitude of the magnetic field and the velocity is given by $V = (u, 0, w)$.

Assumptions of the current research are explained below:

- The time and angular dependence are eliminated, as well as incompressible conditions using steady, incompressible and axisymmetric flow, which simplifies governing equations.

- The electromagnetic fluid that is conducting with a robust magnetic field (including the Hall effect) alters the Lorentz force in the momentum equation.

- Minor magnetic Reynolds number would permit the ignored magnetic field stemming at the applied magnetic field the same.

- Thermal conductivity is temperature dependent, thus making the heat conduction term in the energy equation to change.

- Zero thermoelectric effects correspond to zero electric field and no effect on the flow.

- Cattaneo-Christov heat and mass flux models incorporate a thermal and solutal relaxation time into energy and solute transport equations.

The modified Ohm's law, which accounts to Hall's currents, is represented as follows [31, 32].

$$J + \frac{m}{B_0}(J \times B) = \sigma(V \times B) \tag{1}$$

Where V is fluid velocity, J is current density, B is the induction magnetic vector is a term and $m = \omega_e \tau_e$ is the Hall parameter. We analyzed the equation (1) utilizing the velocity and field magnetic vectors to obtain the Hall flow terms shown below.

$$J \times B = (0)e_r + \left(\frac{\sigma B_0^2 m R^3 w}{r\,(m^2R^2 + r^2)}\right) e_\theta - \left(\frac{\sigma B_0^2 R^2 w}{(m^2R^2 + r^2)}\right) e_z \tag{2}$$

In which e_r, e_θ, and e_z are the dimensions of the standard vectors throughout (r, θ, z) orders, correspondingly.

The governing boundary layer equations of mass conservation, momentum, energy and species transport can be derived as mentioned above with the Williamson fluid using assumptions as listed above and including the Hall current factor (Equation 2), as follow [33–36].

$$\frac{\partial (rw)}{\partial z} + \frac{\partial (ru)}{\partial r} = 0, \tag{3}$$

$$w\frac{\partial w}{\partial z} + u\frac{\partial w}{\partial r} = v\left[\frac{\partial^2 w}{\partial r^2} + \frac{1}{r}\frac{\partial w}{\partial r} + \sqrt{2}\Gamma\frac{\partial w}{\partial r}\frac{\partial^2 w}{\partial r^2} + \frac{\Gamma}{\sqrt{2}r}\left(\frac{\partial w}{\partial r}\right)^2\right] - \frac{\sigma B_0^2 R^2}{\rho\,(m^2R^2 + r^2)}w, \tag{4}$$

$$w\frac{\partial T}{\partial z} + u\frac{\partial T}{\partial r} + \epsilon_1 \Omega_T = \frac{\partial}{\partial r}\left(\alpha r \frac{\partial T}{\partial r}\right)\frac{1}{r} + \frac{(T - T_\infty)}{\rho C_p}Q - \frac{\partial}{\partial r}(rq_r)\frac{1}{\rho C_p} + \tau\left[D_B\frac{\partial T}{\partial r}\frac{\partial C}{\partial r} + \frac{D_T}{T_\infty}\left(\frac{\partial T}{\partial r}\right)^2\right], \tag{5}$$

$$w\frac{\partial C}{\partial z}+u\frac{\partial C}{\partial r}+\epsilon_2\Omega_C= D_B.\frac{1}{r}\frac{\partial}{\partial r}\left(r\frac{\partial C}{\partial r}\right)+\frac{D_T}{T_\infty}\frac{1}{r}\frac{\partial}{\partial r}\left(r\frac{\partial T}{\partial r}\right) - K_r\left(C-C_\infty\right), \tag{6}$$

For the model under consideration, the related boundary conditions

$$\left.\begin{aligned} w=W(z)=\tfrac{U_o z}{l}, u=0, -K_T\tfrac{\partial T}{\partial r}=h_T\left(T_f-T\right), \\ -D_B\tfrac{\partial C}{\partial r}=K_m\left(C_f-C\right)\ at\ r=R, \\ w\to 0,\ C\to C_\infty,\ T\to T_\infty,\ as\ r\to\infty \end{aligned}\right\} \tag{7}$$

By reducing the quantity of variables and converting the equations to ODEs, we simplified the analysis, making it easier to find solutions and get a deeper knowledge of the problem.

$$\begin{aligned} \eta&=\sqrt{\tfrac{U_0}{vl}}\left(\tfrac{r^2-R^2}{2R}\right), & \psi&=f(\eta)\sqrt{\tfrac{vU_0}{l}}Rz, \\ \phi(\eta)&=\tfrac{C-C_\infty}{C_f-C_\infty}, & u&=-f(\eta)\sqrt{\tfrac{vU_0}{l}}\tfrac{R}{r}, \\ \theta(\eta)&=\tfrac{T-T_\infty}{T_f-T_\infty}, & w&=\tfrac{U_0}{l}f'(\eta)z. \end{aligned} \tag{8}$$

In equation (5), the variant thermal conductivity of the fluid is depicted as α. Rosseland approximation to radiation effects is used to get the expression of the temperature-dependent thermal conductivity.

$$\begin{aligned} \alpha&=\alpha_\infty\left(1+\epsilon\theta(\eta)\right), \\ q_r&=-\frac{4\sigma^*}{3K^*}\frac{\partial T^4}{\partial r}. \end{aligned} \tag{9}$$

It can also be expanded as a Taylor series around the reference point T^4 around $T_\infty$with the assumption that there exist a temperature gradient in the flow. When we keep only lower-order terms we are left with T_∞.

$$T^4=4T_\infty^3T-T_\infty^4 \tag{10}$$

Additionally, the following is the formula for the term Ω_T in Equation (5) that is derived using the CCEF model:

$$\begin{aligned} \Omega_T=&w^2\frac{\partial^2T}{\partial z^2}+u^2\frac{\partial^2T}{\partial r^2}+2uw\frac{\partial^2T}{\partial z\partial r}+w\frac{\partial w}{\partial z}\frac{\partial T}{\partial z} \\ &+w\frac{\partial u}{\partial z}\frac{\partial T}{\partial r}+u\frac{\partial w}{\partial r}\frac{\partial T}{\partial z}+u\frac{\partial u}{\partial r}\frac{\partial T}{\partial r} \end{aligned} \tag{11}$$

We obtain the following expression by replacing Equation (5) with Eqs. (9)–(10).

$$\begin{aligned} &w\frac{\partial T}{\partial z}+u\frac{\partial T}{\partial r}+\epsilon_1\left(w^2\frac{\partial^2T}{\partial z^2}+u^2\frac{\partial^2T}{\partial r^2}+2uw\frac{\partial^2T}{\partial z\partial r}\right. \\ &\left.+w\frac{\partial w}{\partial z}\frac{\partial T}{\partial z}+w\frac{\partial u}{\partial z}\frac{\partial T}{\partial r}+u\frac{\partial w}{\partial r}\frac{\partial T}{\partial z}+u\frac{\partial u}{\partial r}\frac{\partial T}{\partial r}\right)= \\ &\frac{\partial}{\partial r}\left(\alpha r\frac{\partial T}{\partial r}\right)\frac{1}{r}+\frac{(T-T_\infty)}{\rho c_p}Q-\frac{1}{\rho C_p}\left(\frac{\partial q_r}{\partial r}+\frac{1}{r}q_r\right) \\ &+\tau\left[D_B\frac{\partial T}{\partial r}\frac{\partial C}{\partial r}+\frac{D_T}{T_\infty}\left(\frac{\partial T}{\partial r}\right)^2\right], \end{aligned} \tag{12}$$

The formula for the term Ω_C in Equation (6), which is derived from the Cattaneo-Christov mass flux model, is

$$\begin{aligned} \Omega_C=&w^2\frac{\partial^2C}{\partial z^2}+u^2\frac{\partial^2C}{\partial r^2}+2uw\frac{\partial^2C}{\partial z\partial r}+w\frac{\partial w}{\partial z}\frac{\partial c}{\partial z} \\ &+w\frac{\partial u}{\partial z}\frac{\partial C}{\partial r}+u\frac{\partial w}{\partial r}\frac{\partial C}{\partial z}+u\frac{\partial u}{\partial r}\frac{\partial C}{\partial r} \end{aligned} \tag{13}$$

The updated concentration equation that results from applying Equation (13) to Equation (6) is as follows:

$$\begin{aligned} &w\frac{\partial C}{\partial z}+u\frac{\partial C}{\partial r}+\epsilon_2\left(w^2\frac{\partial^2C}{\partial z^2}+u^2\frac{\partial^2C}{\partial r^2}+2uw\frac{\partial^2C}{\partial z\partial r}\right. \\ &\left.+w\frac{\partial w}{\partial z}\frac{\partial c}{\partial z}+w\frac{\partial u}{\partial z}\frac{\partial C}{\partial r}+u\frac{\partial w}{\partial r}\frac{\partial C}{\partial z}+u\frac{\partial u}{\partial r}\frac{\partial C}{\partial r}\right)= \\ &D_B.\frac{1}{r}\frac{\partial}{\partial r}\left(r\frac{\partial C}{\partial r}\right)+\frac{D_T}{T_\infty}\frac{1}{r}\frac{\partial}{\partial r}\left(r\frac{\partial T}{\partial r}\right)-K_r\left(C-C_\infty\right) \end{aligned} \tag{14}$$

Under the applied similarity transformations, the continuity equation is maintained. These transformations convert Eqs. (4), (12), and (14) to the following ODEs.

$$\begin{aligned} &(1+2\eta\gamma)f'''+ff''-\left(f'\right)^2+2\gamma f''+\frac{3}{2}(1+2\eta\gamma)^{\frac{1}{2}}\gamma\lambda\left(f''\right)^2 \\ &+\lambda(1+2\eta\gamma)^{\frac{3}{2}}f''f'''-\left(\frac{M^2}{m^2+(1+2\eta\gamma)}\right)f'=0, \end{aligned} \tag{15}$$

$$
\begin{aligned}
&(1+2\eta\gamma)\left((1+\epsilon\theta)\frac{4}{3}Rd\right)\theta'' + (\theta')^2(1+2\eta\gamma)\epsilon \\
&+\left(Prf+2\gamma+2\epsilon\gamma\theta+\frac{8}{3}Rd\gamma\right)\theta' \\
&-Pr\lambda_t\left((f)^2\theta'' + ff'\theta'\right)+Pr\beta\theta \\
&+(1+2\eta\gamma)\,\mathrm{Pr}\left(Nb\theta'\phi'+Nt\theta'^2\right)=0,
\end{aligned}
\tag{16}
$$

$$
\begin{aligned}
&(1+2\eta\gamma)\left(\phi''+\frac{Nt}{Nb}\theta''\right)+2\gamma\left(\phi'+\frac{Nt}{Nb}\theta'\right) \\
&-Sc\lambda_c\left((f)^2\phi''+ff'\phi'\right)+Scf\phi'-ScK\phi=0.
\end{aligned}
\tag{17}
$$

In Non-dimensional parameters are: where $Pr = \frac{\nu}{\alpha_\infty}$, is the Prandtl number $\alpha_\infty = \frac{k}{\rho C_p}$, thermal conductivity $\gamma = \sqrt{\frac{\nu l}{U_0 R^2}}$ is the Curvature parameter, $Rd = 4\frac{\sigma^*}{K^*}\frac{T_\infty^3}{k}$ is the thermal radiation, $Nb = \frac{\tau D_B\left(C_f - C_\infty\right)}{\nu}$ Brownian motion, $K = \frac{K_r l}{U_0}$ represent chemical reaction parameter, $Nt = \frac{\tau D_T\left(T_f - T_\infty\right)}{\nu T_\infty}$ is the thermophoresis parameter, and $\lambda = \frac{\sqrt{2}\Gamma U_0^{\frac{3}{2}} z}{\nu^{\frac{1}{2}} l^{\frac{3}{2}}}$ is the Weissenberg number The parameters for the magnetic field $M^2 = \frac{\sigma B_0^2 l}{U_0 \rho}$, heat generation are $\beta = \frac{Ql}{\rho C_p U_0}$, Lewis number is $Le = \frac{\alpha_\infty}{D_B}$ and the Schmidt number is $Sc = PrLe$.

Boundary condition given as follow Jakhar et al. [40].

$$
\left.
\begin{gathered}
f'(0)=1, f(0)=0, \\
\theta'(0)+(Bi)_1\left(1-\theta(0)\right)=\phi'(0)+(Bi)_2\left(1-\phi(0)\right)=0, \\
\theta(\eta)\to 0, \phi(\eta)\to 0,\ f'(\eta)\to 0\ \ as\ \ \eta\to\infty
\end{gathered}
\right\}
\tag{18}
$$

While $(Bi)_1$ and $(Bi)_2$ are actually the temperature & concentrations Biot numbers, respectively.

Skin friction, locally Nusselt number, and Sherwood number are physical properties. There will be bodily expression:

$$
\begin{aligned}
C_f &= \frac{\tau_w}{\rho U^2}, \\
Nu &= \frac{r q_r}{k\left(T_s - T_\infty\right)}, \\
Sh &= \frac{r j_r}{D_B\left(C_s - C_\infty\right)}.
\end{aligned}
\tag{19}
$$

where,

$$
\begin{aligned}
\tau_w &= \mu\left(\frac{\partial w}{\partial r}+\Gamma\frac{\partial w}{\partial r}\frac{\partial w}{\partial r}\right), \\
q_r &= -k\frac{\partial T}{\partial r}, \\
j_r &= -D_B\frac{\partial C}{\partial r}\ \text{at}\ r=R
\end{aligned}
\tag{20}
$$

Dimensionless versions of the preceding statements are expressed as follows.

$$
\begin{aligned}
\frac{\sqrt{Re}C_f}{2} &= \tfrac{\lambda}{2}f''(0)^2 + f''(0), \\
\sqrt{Re}\,Nu &= -\left(1+\tfrac{4}{3}Rd\right)\Theta'(0), \\
\sqrt{Re}\,Sh &= -\varphi'(0).
\end{aligned}
\tag{21}
$$

3 Methodology

The nonlinear model problem (15)-(17) involving modeling boundary condition (18) was solved using the Optimal Homotopy Analysis Method (OHAM) [41–46]. The solution procedure follows the computational algorithm depicted in Figure 2. Suppose $\eta = \varpi$. These initial beliefs were originally specified:

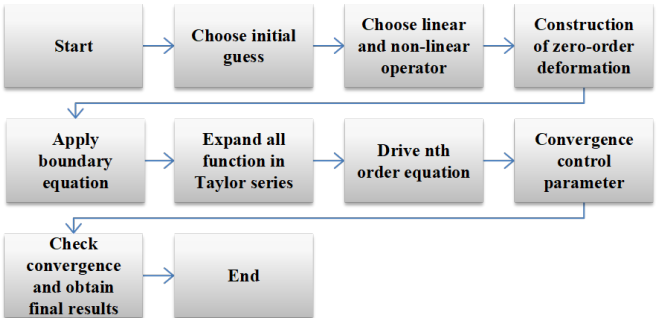

Figure 2. Flow chart for optimal homotopy analysis method.

$$
\begin{aligned}
f_o(\varpi) &= 1-e^{-\varpi}, \\
\theta_o(\varpi) &= \left(\frac{Bi_1}{1+Bi_1}\right)e^{-\varpi}, \\
\phi_0(\varpi) &= \left(\frac{Bi_2}{1+Bi_2}\right)e^{-\varpi}.
\end{aligned}
\tag{22}
$$

The $\mathcal{L}_f, \mathcal{L}_\theta\ and\ \mathcal{L}_\phi$ are linear operators, which are perceived as

$$
\mathcal{L}_f(f) = f''' - f',\ \mathcal{L}_\theta(\theta) = \theta'' - \theta,\ \mathcal{L}_\phi(\phi) = \phi'' - \phi, \tag{23}
$$

Which possess following attributes:

$$\begin{gathered}\mathcal{L}_f\left(\alpha_1+\alpha_2 e^{-\varpi}+\alpha_3 e^{\varpi}\right)=0,\\ \mathcal{L}_\theta\left(\alpha_4 e^{-\varpi}+\alpha_5 e^{\varpi}\right)=0,\ \ \mathcal{L}_\phi\left(\alpha_6 e^{-\varpi}+\alpha_7 e^{\varpi}\right)=0.\end{gathered} \tag{24}$$

where α are constant coefficient.

The $\aleph_f, \aleph_\theta \; and \; \aleph_\phi$are Nonlinear operator expressed by

$$\begin{aligned}&\aleph_f\left[f\left(\mathcal{R};\varpi\right)\right]=(1+2\eta\gamma)\frac{\partial^3 f\left(\mathcal{R};\varpi\right)}{\partial\varpi^3}\\&+f\left(\mathcal{R};\psi\right)\frac{\partial^2 f\left(\mathcal{R};\varpi\right)}{\partial\varpi^2}-\left(\frac{\partial f\left(\mathcal{R};\varpi\right)}{\partial\varpi}\right)^2\\&+(2\gamma)\frac{\partial^2 f\left(\mathcal{R};\varpi\right)}{\partial\varpi^2}+\frac{3}{2}(1+2\eta\gamma)^{\frac{1}{2}}\gamma\lambda\left(\frac{\partial^2 f\left(\mathcal{R};\varpi\right)}{\partial\varpi^2}\right)^2\\&+\lambda(1+2\eta\gamma)^{\frac{3}{2}}\frac{\partial^2 f\left(\mathcal{R};\varpi\right)}{\partial\varpi^2}\frac{\partial^3 f\left(\mathcal{R};\varpi\right)}{\partial\varpi^3}\\&-\left(\frac{M^2}{m^2+(1+2\eta\gamma)}\right)\frac{\partial f\left(\mathcal{R};\varpi\right)}{\partial\varpi},\end{aligned} \tag{25}$$

$$\begin{aligned}&\aleph_\theta\left[\theta\left(\mathcal{R};\varpi\right),\phi\left(\mathcal{R};\varpi\right)\right]=\\&\left((1+\epsilon\theta)\frac{4}{3}Rd\right)\frac{\partial^2\theta\left(\mathcal{R};\varpi\right)}{\partial\varpi^2}(1+2\eta\gamma)\\&+\left(Prf+2\gamma+2\epsilon\gamma\theta+\frac{8}{3}Rd\gamma\right)\frac{\partial\theta\left(\mathcal{R};\varpi\right)}{\partial\varpi}\\&+\epsilon(1+2\eta\gamma)\left(\frac{\partial\theta\left(\mathcal{R};\varpi\right)}{\partial\varpi}\right)^2\\&+(1+2\eta\gamma)\,\mathrm{Pr}\left[(Nb)\frac{\partial\theta\left(\mathcal{R};\varpi\right)}{\partial\varpi}\frac{\partial\phi\left(\mathcal{R};\varpi\right)}{\partial\varpi}+Nt\left(\frac{\partial\theta\left(\mathcal{R};\varpi\right)}{\partial\varpi}\right)^2\right]\\&-Pr\lambda_t\left[f^2\frac{\partial^2\theta\left(\mathcal{R};\varpi\right)}{\partial\varpi^2}+f\left(\mathcal{R};\psi\right)\frac{\partial f\left(\mathcal{R};\varpi\right)}{\partial\varpi}\frac{\partial\theta\left(\mathcal{R};\varpi\right)}{\partial\varpi}\right]\\&+\left((Pr\beta)\right)\theta\left(\mathcal{R};\varpi\right),\end{aligned} \tag{26}$$

$$\begin{aligned}&\aleph_\phi\left[\theta\left(\mathcal{R};\varpi\right),\phi\left(\mathcal{R};\varpi\right)\right]=\\&2\gamma\left(\frac{\partial\phi\left(\mathcal{R};\varpi\right)}{\partial\varpi}+\frac{Nt}{Nb}\frac{\partial\theta\left(\mathcal{R};\varpi\right)}{\partial\varpi}\right)\\&+(1+2\eta\gamma)\left(\frac{\partial^2\phi\left(\mathcal{R};\varpi\right)}{\partial\varpi^2}+\frac{Nt}{Nb}\frac{\partial^2\theta\left(\mathcal{R};\varpi\right)}{\partial\varpi^2}\right)\\&-(Sc*\lambda_c)\left[f^2\frac{\partial^2\phi\left(\mathcal{R};\varpi\right)}{\partial\varpi^2}+f\left(\mathcal{R};\varpi\right)\frac{\partial f\left(\mathcal{R};\varpi\right)}{\partial\varpi}\frac{\partial\phi\left(\mathcal{R};\varpi\right)}{\partial\varpi}\right]\\&+(Sc)f\left(\mathcal{R};\varpi\right)\frac{\partial\phi\left(\mathcal{R};\varpi\right)}{\partial\varpi}-(KSc)\phi\left(\mathcal{R};\varpi\right).\end{aligned} \tag{27}$$

Zeroth-order problems are defined as:

$$\begin{aligned}&(1-\mathcal{R})\ \mathcal{L}_f\left[f\left(\mathcal{R};v\right)-f_o(\varpi)\right]\\&=\mathcal{R}\hbar_f\aleph_f\left[f\left(\mathcal{R};\varpi\right),g\left(\mathcal{R};\varpi\right)\right],\end{aligned} \tag{28}$$

$$\begin{aligned}&(1-\mathcal{R})\ \mathcal{L}_\theta\left[\theta\left(\mathcal{R};\varpi\right)-\theta_o(\varpi)\right]\\&=\mathcal{R}\hbar_\theta\aleph_\theta\left[\theta\left(\mathcal{R};\varpi\right),\phi\left(\mathcal{R};\varpi\right)\right],\end{aligned} \tag{29}$$

$$\begin{aligned}&(1-\mathcal{R})\ \mathcal{L}_\phi\left[\phi\left(\mathcal{R};\varpi\right)-\phi_o(\varpi)\right]\\&=\mathcal{R}\hbar_\phi\aleph_\phi\left[\theta\left(\mathcal{R};\varpi\right),\phi\left(\mathcal{R};\varpi\right)\right].\end{aligned} \tag{30}$$

The corresponding B.C are

$$\begin{gathered}\left.\frac{\partial f(\mathcal{R};\varpi)}{\partial\varpi}\right|_{\varpi\to\infty}=0,\quad\left.\frac{\partial f(\mathcal{R};\varpi)}{\partial\varpi}\right|_{\varpi=0}=0,\quad f\left(\mathcal{R};\varpi\right)|_{\varpi=0}=0,\\ \theta\left(\mathcal{R};\varpi\right)|_{\varpi\to\infty}=0,\quad\left.\frac{\partial\theta(\mathcal{R};\varpi)}{\partial\varpi}\right|_{\varpi=0}=-Bi_1(1-\theta),\\ \phi\left(\mathcal{R};\varpi\right)|_{\varpi\to\infty}=0,\ \ \phi\left(\mathcal{R};\varpi\right)|_{\varpi=0}=-Bi_2(1-\phi).\end{gathered} \tag{31}$$

The variables which are used to govern the method's stability are $\hbar_f$, $\hbar_\theta$ and $\hbar_\phi$ while $\mathcal{R}\in[0,1]$ acts as the placing factor.

$$\begin{gathered}f(\varpi;0)=f_o(\varpi),\ \ f(\varpi;1)=f(\varpi)\\ \theta(\varpi;0)=\theta_o(\varpi),\ \ \theta(\varpi;1)=\theta(\varpi)\\ \phi(\varpi;0)=\phi_o(\varpi),\ \ \phi(\varpi;1)=\phi(\varpi)\end{gathered} \tag{32}$$

Taylor's serial extension includes:

$$\begin{gathered}f\left(\mathcal{R};\varpi\right)=f_o(\varpi)+\textstyle\sum_{n=1}^{\infty}f_n(\varpi)\mathcal{R}^n,\\ \theta\left(\mathcal{R};\varpi\right)=\theta_o(\varpi)+\textstyle\sum_{n=1}^{\infty}\theta_n(\varpi)\mathcal{R}^n,\\ \phi\left(\mathcal{R};\varpi\right)=\phi_o(\varpi)+\textstyle\sum_{n=1}^{\infty}\phi_n(\varpi)\mathcal{R}^n,\end{gathered} \tag{33}$$

where,

$$\begin{aligned}f_n(\varpi)&=\frac{1}{n!}\left.\frac{\partial f\left(\mathcal{R};\varpi\right)}{\partial\varpi}\right|_{\mathcal{R}=0'},\\ \theta_n(\varpi)&=\frac{1}{n!}\left.\frac{\partial\theta\left(\mathcal{R};\varpi\right)}{\partial\varpi}\right|_{\mathcal{R}=0},\\ \phi_n(\varpi)&=\frac{1}{n!}\left.\frac{\partial\phi\left(\mathcal{R};\varpi\right)}{\partial\varpi}\right|_{\mathcal{R}=0}\end{aligned} \tag{34}$$

The secondary restrictions $\hbar_f$, $\hbar_\theta$, $\hbar_\phi$ are labelled. After changing $\mathcal{R}=1$ in (33), we get

$$\begin{gathered}f(\varpi)=f_o(\varpi)+\textstyle\sum_{n=1}^{\infty}f_n(\varpi),\\ \theta(\varpi)=\theta_o(\varpi)+\textstyle\sum_{n=1}^{\infty}\theta_n(\varpi),\\ \phi\left(\varpi\right)=\phi_o(\varpi)+\textstyle\sum_{n=1}^{\infty}\phi_n(\varpi),\end{gathered} \tag{35}$$

n^{th} order problem state the following

$$\begin{gathered}\mathcal{L}_f\left[f_n(\varpi)-\mathbb{C}_n f_{n-1}(\varpi)\right]=\hbar_f\mathcal{X}_n^f(\varpi),\\ \mathcal{L}_\theta\left[\theta_n(\varpi)-\mathbb{C}_n\theta_{n-1}(\varpi)\right]=\hbar_\theta\mathcal{X}_n^\theta(\varpi),\\ \mathcal{L}_\phi\left[\phi_n(\varpi)-\mathbb{C}_n\phi_{n-1}(\varpi)\right]=\hbar_\phi\mathcal{X}_n^\phi(\varpi).\end{gathered} \tag{36}$$

Boundary condition are

$$\begin{aligned} f'(\infty) = f'(0) + 1 = f(0) = 0, \\ \theta'(0) + Bi_1\,(1 - \theta(0)) = \theta(\infty) = 0, \\ \phi'(0) + Bi_2\,(1 - \phi(0)) = \phi(\infty) = 0. \end{aligned} \tag{37}$$

here,

$$\begin{aligned} &\mathcal{X}_n^f(\varpi) = (1+2\eta\gamma){f'''}_{n-1} + f{f''}_{n-1} - \left({f'}_{n-1}\right)^2 \\ &+ 2\gamma{f''}_{n-1} + \frac{3}{2}(1+2\eta\gamma)^{\frac{1}{2}}\gamma\lambda \\ &\left({f''}_{n-1}\right)^2 + \lambda(1+2\eta\gamma)^{\frac{3}{2}}\left(\sum_{m=0}^{n-1}{f''}_{n-1}{f'''}_{m}\right) \\ &- \left(\frac{M^2}{m^2+(1+2\eta\gamma)}\right){f'}_{n-1} = 0 \end{aligned} \tag{38}$$

$$\begin{aligned} &\mathcal{X}_n^\theta(\varpi) = \left((1+\epsilon\theta)\frac{4}{3}Rd\right){\theta''}_{n-1}(1+2\eta\gamma) \\ &+ \left(Prf + 2\gamma + 2\epsilon\gamma\theta + \frac{8}{3}Rd\gamma\right){\theta'}_{n-1} \\ &+ \left({\theta'}_{n-1}\right)^2\epsilon(1+2\eta\gamma) - Pr\lambda_t\left(f^2{\theta''}_{n-1} + ff'{\theta'}_{n-1}\right) \\ &+ (Pr\beta)\theta + (1+2\eta\gamma)\,\mathrm{Pr} \\ &\left[Nb\left(\sum_{m=0}^{n-1}{\theta'}_{n-1-m}{\phi'}_{m}\right) + Nt\left({\theta'}_{n-1}\right)^2\right] = 0, \end{aligned} \tag{39}$$

$$\begin{aligned} &\mathcal{X}_n^\phi(\varpi) = 2\gamma\left({\phi'}_{n-1} + \frac{Nt}{Nb}{\theta'}_{n-1}\right) \\ &+ (1+2\eta\gamma)\left({\phi''}_{n-1} + \frac{Nt}{Nb}{\theta''}_{n-1}\right) - Sc\lambda_c \\ &\left(f^2{\phi''}_{n-1} + f\left(\sum_{m=0}^{n-1}{\phi'}_{n-1-m}{f'}_{m}\right)\right) \\ &+ Scf{\phi'}_{n-1} - KSc\phi = 0. \end{aligned} \tag{40}$$

where,

$$\mathbb{C}_n = \begin{cases} 0\ if\ \mathcal{R} \leq 1 \\ 1\ if\ \mathcal{R} > 1 \end{cases} \tag{41}$$

4 Results and Discussion

In this analysis carried on the flow of a Williamson fluid flowing over a stretched cylindrical surface due to an externally applied magnetic field. The paper takes into account combined effects of Curvature parameter, Weissenberg number, Time relaxation Parameter, Hall current, Magnetic field, Thermal conductivity, Prandtl number, Radiation Parameter, Heat generation, and Schmidt number, Thermophoresis parameter, Brownian motion, chemical reactions and Biot number all of which have substantial influence in the flow profile. The influence of the existence of a magnetic field and non-Newtonian fluid properties implements a complicated interaction, but this fact influences no velocity, temperature, and concentration distributions. The profile shown in the graph below is generated with Mathematica software along the cylinder and shows how the effect of the magnetic forces, thermal gradients and chemical processes affect the overall performance of the flow. The visualization is an important insight on how physical effects interact in magnetohydrodynamic systems with non-Newtonian fluids. For the analysis, key physical parameters are chosen as follows [39, 40]: $\gamma(0.0 \leq 1.0)$, $\lambda(0.0 \leq 1.0)$, $\lambda_t(0.0 \leq 2.0)$, $\lambda_c(0.0 \leq 4)$, $m(0.4 \leq 0.5)$, $M(0.0 \leq 1.0)$, $\epsilon(0.0 \leq 1.5)$, $Pr(1.0 \leq 4.0)$, $Rd(1.0 \leq 4.0)$, $\beta(0.1 \leq 0.3)$, $Sc(0.1 \leq 1.0)$, $Nt(1.0 \leq 4.0)$, $Nb(1.0 \leq 4.0)$, $K(0.0 \leq 0.1)$ and $Bi(0.0 \leq 1.0)$.

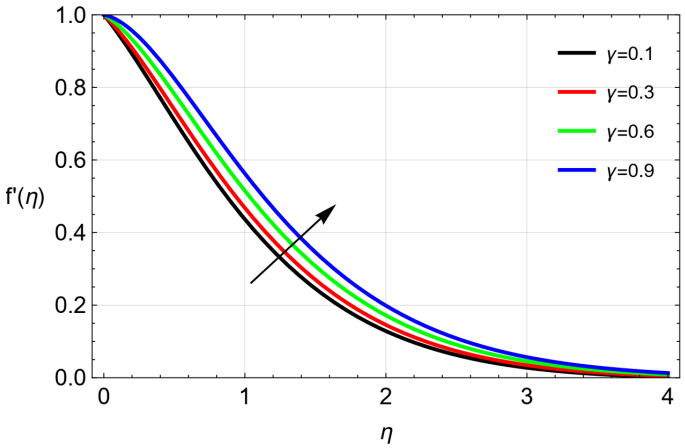

Figure 3. Plot the graph of curvature parameter γ on $f'(\eta)$.

As the plots in Figures 3, 4 and 5 indicate, the curvature parameter γ has significant effect on the velocity, concentration and temperature profiles of the fluid. As γ, corresponding to a curvier cylinder surface, increases, there is higher velocity, concentration and a drop in temperature. The increase of the velocity can be explained by less resistance in the flow path, enabling easier movement of the fluid and transfer of momentum. This increases in its turn mass transport, raising the concentration of fluid close to the surface. This cooling effect comes due to the fact

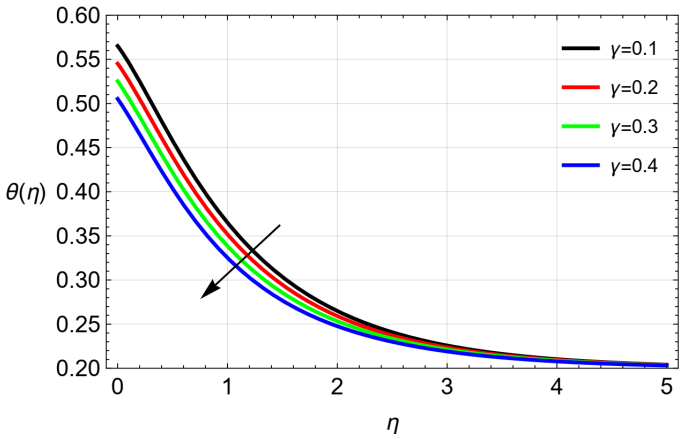

Figure 4. Plot the graph curvature parameter γ on temperature.

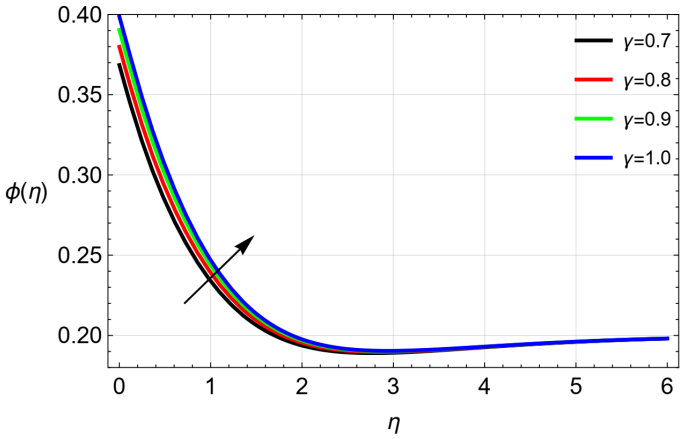

Figure 5. Plot the graph curvature parameter γ on concentration.

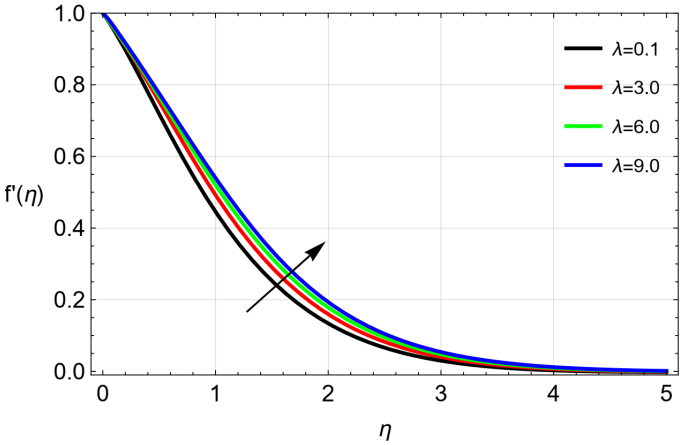

Figure 6. Plot the graph Weissenberg number λ on $f'(\eta)$.

that a much larger curvature increases the surface area between the cylinder and the fluid it is exposed to. This enhances improved thermal conduction and convective heat transfer and the boundary layer is cooled. In general, the curvature parameter, is essential in dynamically, diffusively and thermally configuring the fluid, providing useful control of transports along curved forms.

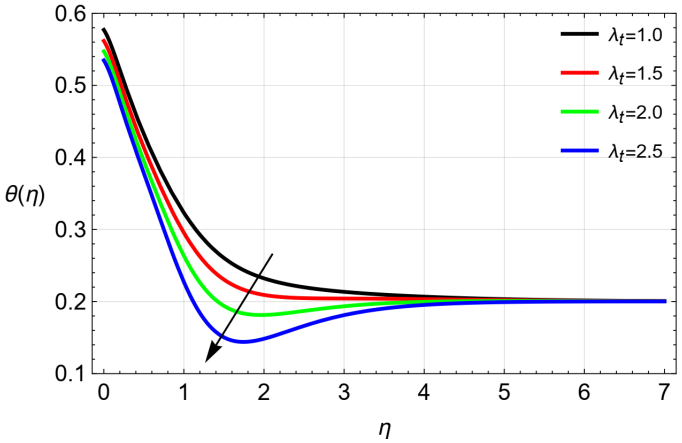

Figure 7. Plot the graph Thermal relaxation parameter λ_t on temperature.

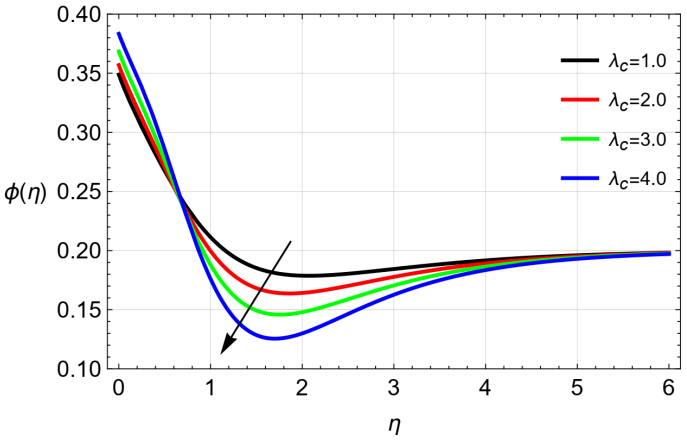

Figure 8. Plot the graph Soultal relaxation parameter λ_c on temperature.

Figure 6 shows that as the Weissenberg number λ fluid increases, it will enhance fluid velocity. Greater values imply longer relaxation periods, in that the fluid acts more elastically. In Williamson fluids, increased elasticity enables the fluid to resist deformation, to flow more rapidly. This flexibility also enhances the process of overcoming magnetic resistive forces in a system to more velocity in the MHD systems. Therefore, an advanced value of Weissenberg numbers enhances fluid flow and better flow pattern. Figures 7 and 8 show the thermal and concentration relaxation parameters (λ_t and λ_c), which represent heat and mass transfer rates, respectively. Increased λ_t causes the system to take longer to react to thermal changes, resulting in better heat dissipation with a slower temperature decrease. Higher λ_c slows the changing to the concentration field, causing mass accumulation

and increasing concentration. In summary, higher λ_t values lower temperature and increase concentration. Understanding these mechanisms provides more information on the system's thermal as well as mass transport behavior.

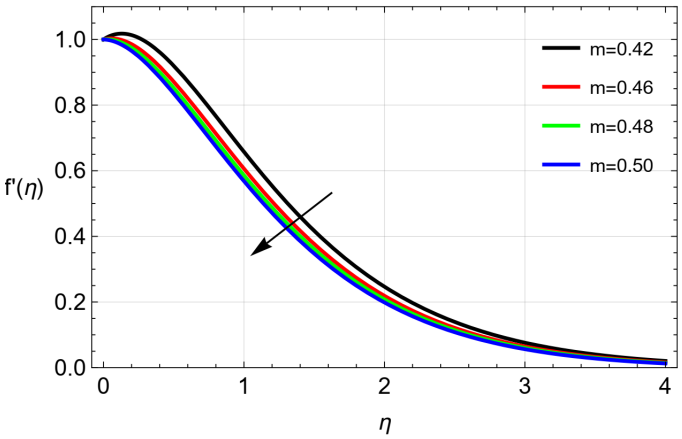

Figure 9. Plot the graph Hall current m on $f'(\eta)$.

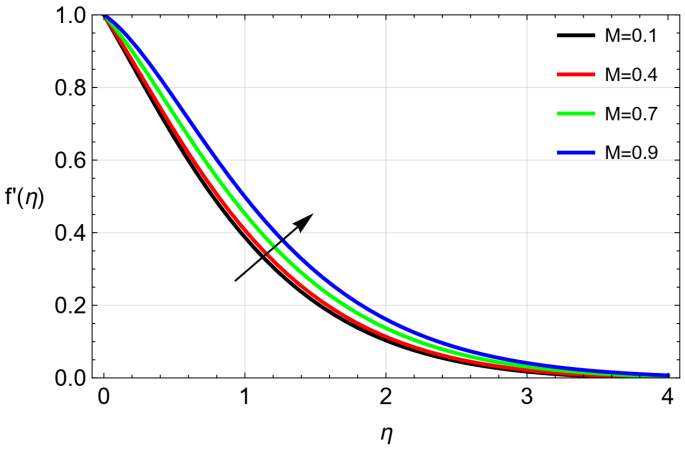

Figure 10. Plot the graph Magnetic field M on $f'(\eta)$.

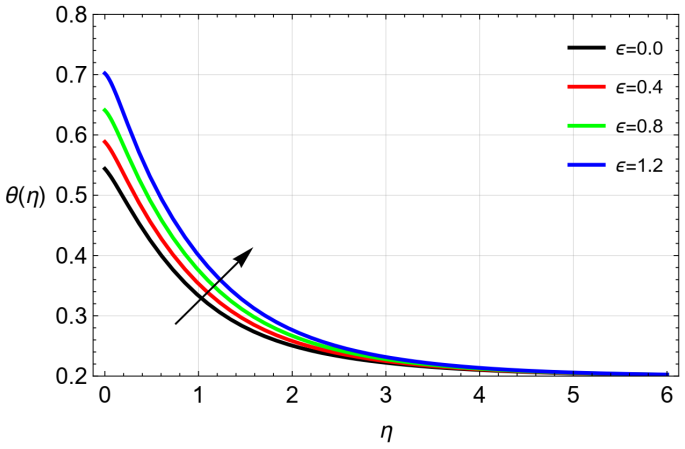

Figure 11. Plot the graph thermal conductivity ϵ on temperature.

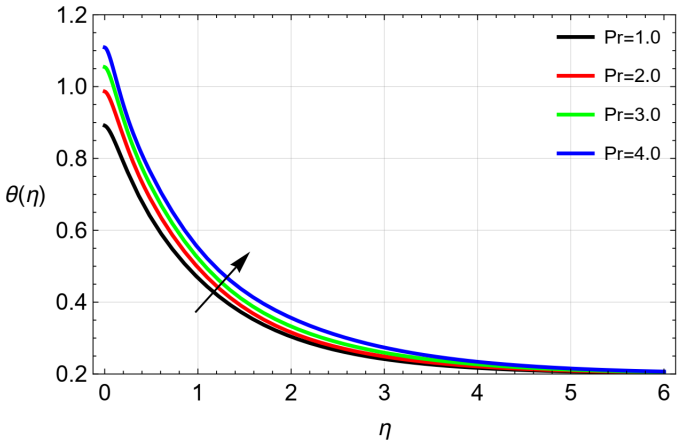

Figure 12. Plot the graph Prandtl number Pr on temperature.

Figure 9 shows that a reduction in Hall parameter m reduces the effect of the magnetic field on the fluid. This decreases the contact of the magnetic field to the fluid particles causing a decrease in velocity. In a lower Hall effect, there is a reduced strength capability to oppose or aid the movement of the fluid; hence movement is slower. An awareness of these physical impacts can aid in interpretation of the behavior of the system in different magnetic impact. Figure 10 shows that the magnetic field exerts more resistance on the flow of fluid as the strength of the magnetic field parameter, M increases. This is because of higher Lorentz force which resists the motion causing the reduction of the velocity. In understanding this mechanism, it figuratively gives more insight into the nature of magnetic effect on fluid behavior. Figure 11 exhibits that increasing the thermal conducting parameter ϵ results in lower fluid temperature due to greater dissipation of heat. This improved thermal conduction causes heat to move away from the liquid more quickly. Understanding this tendency helps to explain the system's thermal response under different conductivity circumstances. The Prandtl number (Pr) in Figure 12 is a dimensionless quantity which is an infrahed of momentum diffusion (viscosity) to thermal diffusion. The more Pr gets, the thicker the fluid is as compared to its capability to transfer heat. This combined with the fact that it causes the fluid to have a thinner thermal boundary layer resulting in increase in heat transfer between the fluid and the surroundings. As a result, there is an increased amount of heat that is held in the fluid, thus elevating the temperature. Therefore, thick fluids have a higher Prandtl number which means that they are more heated because they are less efficiently diffusing thermally.

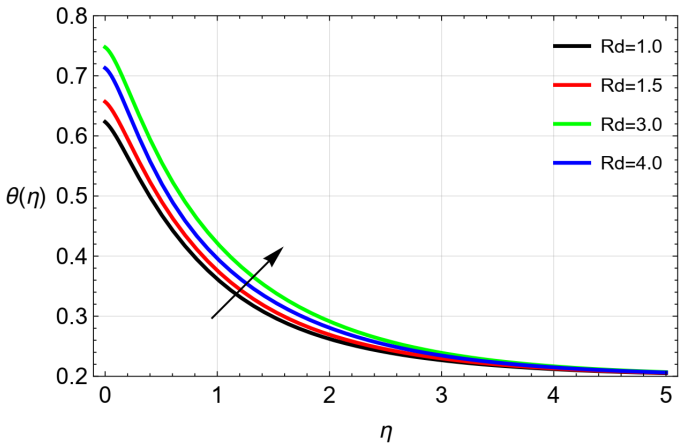

Figure 13. Plot the graph Thermal Radiation Rd on temperature.

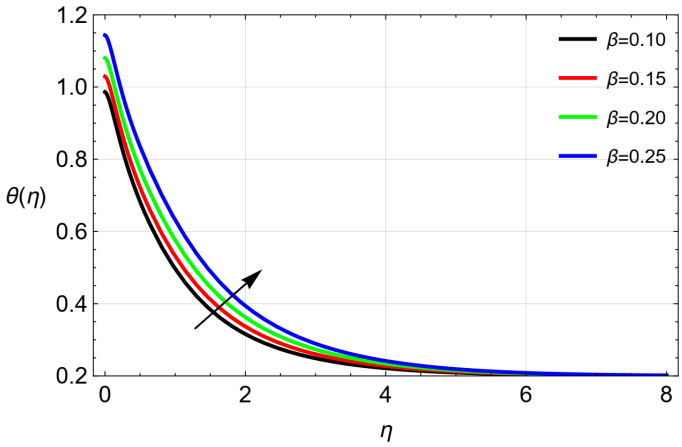

Figure 14. Plot the graph heat generation β on temperature.

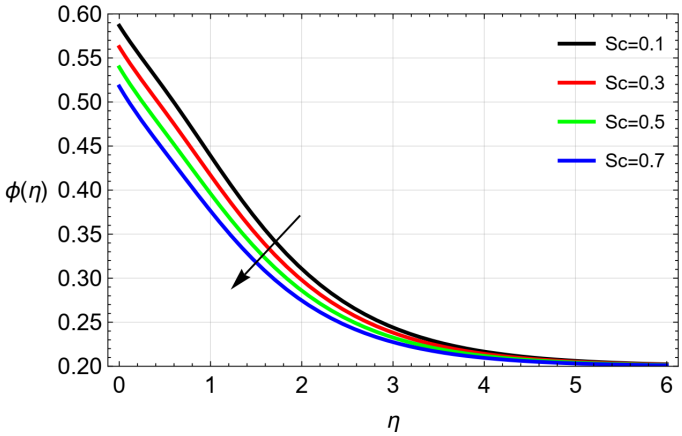

Figure 15. Plot the graph Schmidt number Sc on concentration.

In Figure 13, the radiation parameter Rd influences temperature by determining when the fluid takes and emits thermal radiation. A greater Rd enhances absorption, which causes the fluid to heat up more quickly. At the exact time, emissivity regulates heat loss; more emissivity results in faster cooling, whereas low emissivity induces heat retention. In order the radiation parameter affects either the cooling and heating processes, influencing overall temperature behavior. Figure 14 shows the heat generation parameter β, which governs the quantity of heat produced by the system. Higher β values cause a quicker increase in temperature through increased heat generation, assuming minor cooling effects. Understanding this helps to explain how energy sources influence the system's thermal behavior. As shown in Figure 15, Schmidt number Sc (which is a ratio of momentum diffusivity to mass diffusivity) has an influence on the concentration profile. An increase in Sc will lead to higher concentration gradient and more concentrated at a few locations, whereas the decrease in Sc will lead to a flattening out of concentration and increase in mass diffusion. The knowledge of this can explain the effects of diffusion rates on the pattern of concentrations.

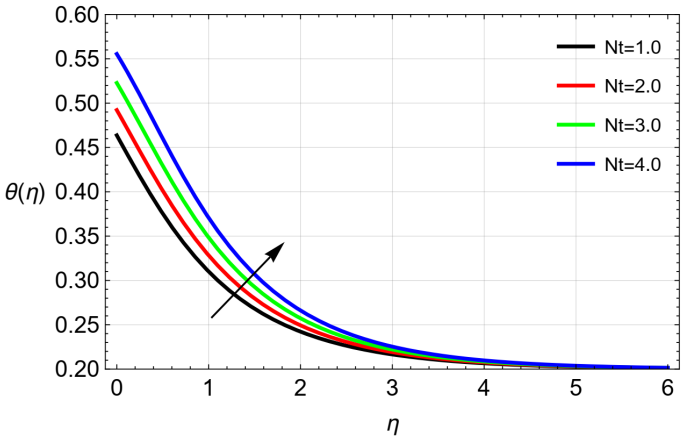

Figure 16. Plot the graph thermophoresis Nt on temperature.

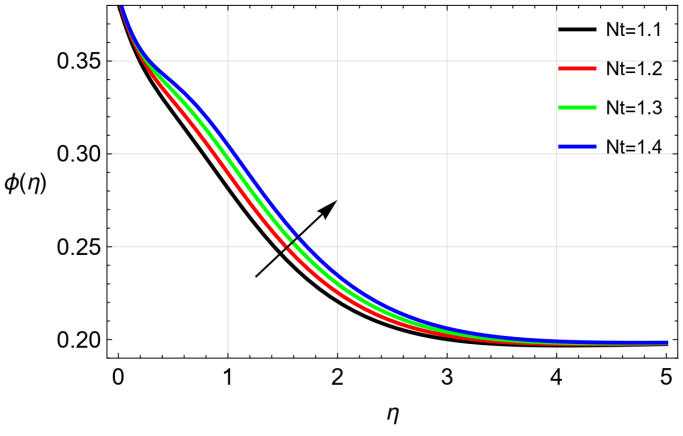

Figure 17. Plot the graph thermophoresis Nt on concentration.

Table 1. Calculated values for Skin friction on $M = 0,\ m = 0\ and\ \gamma = 0$ with respect to λ.

λ	C_f Nadeem et al. [37]	C_f Malik et al. [38]	C_f Bilal et al. [39]	C_f Jakhar et al. [40]	C_f present results
0.0	1	1.005	1.0053	1.002	1.00000000
0.1	0.976558	0.965285	0.965283	0.9811	0.99950198
0.2	0.939517	0.927877	0.927874	0.9606	0.97924993

Table 2. Computational values for Skin friction at $\epsilon = 0.3, (Bi)_1 = 0.2,\ (Bi)_2 = 0.2,\ Rd = 0.4,$ $K = 0.2,\ Sc = 3,\ Pr = 3,\ Nt = 0.2,\ Nb = 0.2.$

γ	λ	M	m	C_f Jakhar et al. [40]	C_f Present Results
0.1	0.4	0.3	0.2	0.9973	0.99636214
0.5	-	-	-	1.0745	1.0550189
1.0	-	-	-	1.1901	1.1349401
0.3	0.1	-	-	1.1183	1.1156701
-	0.3	-	-	1.0600	1.0802283
-	0.5	-	-	0.9799	0.9487434
-	-	0.3	-	1.0246	1.0579687
-	-	0.5	-	1.0719	1.0590739
-	-	0.7	-	1.1374	1.1572667
-	-	-	0.1	1.0253	1.0590658
-	-	-	0.5	1.0208	1.0590853

Figures 16 and 17 allow temperature-directed movement of particle flow by using a thermophoresis parameter Nt. Increasing levels of Nt increases the mobility of the particles towards cooler areas which

Table 3. Numerical values for Nu at $m = 0.2, M = 0.3,\ \lambda = 0.4,\ \gamma = 0.3, (Bi)_1 = 0.2,\ (Bi)_2 = 0.2,\ K = 0.2,\ Sc = 3.$

ϵ	Rd	Pr	β	γ	Nb	Nt	Nu Jakhar et al. [40]	Nu present result
0.0	0.4	0.2	0.1	0.3	0.2	0.5	0.2194	0.2148009
0.5	-	-	-	-	-	-	0.2146	0.230410
1.0	-	-	-	-	-	-	0.2094	0.2303418
0.5	0.0	-	-	-	-	-	0.1519	0.1971689
-	0.3	-	-	-	-	-	0.1999	0.2172685
-	1.0	-	-	-	-	-	0.2956	0.2869087
-	-	0.71	-	-	-	-	0.1710	0.1836760
-	-	7.0	-	-	-	-	0.2570	0.2690744
-	-	-	0.15	-	-	-	0.1478	0.1337890
-	-	-	0.20	-	-	-	0.2837	0.2978369
-	-	-	-	1.0	-	-	0.2162	0.2292780
-	-	-	-	0.5	-	-	0.2248	0.2367901
-	-	-	-	1.0	-	-	0.2388	0.2317825
-	-	-	-	-	0.5	-	0.2119	0.2145402
-	-	-	-	-	1.0	-	0.2074	0.2098388
-	-	-	-	-	1.5	-	0.2028	0.2098374
-	-	-	-	-	-	0.2	0.2191	0.21309419
-	-	-	-	-	-	0.1	0.2057	0.29090422

Table 4. Calculated values for Sh at $\gamma = 0.3, M = 0.3, m = 0.2, (Bi)_1 = 0.2,\ (Bi)_2 = 0.2,\ \lambda = 0.4$.

K	Sc	γ	Nt	Nb	Sh Jakhar et al. [40]	Sh Present results
0.1	3.0	0.3	0.2	0.2	0.1697	0.1658207
0.5	-	-	-	-	0.1785	0.1738265
1.6	-	-	-	-	0.1829	0.1883175
0.2	0.78	-	-	-	0.1478	0.1442373
-	0.96	-	-	-	0.1525	0.1559409
-	2.0	-	-	-	0.1668	0.1658243
-	-	0.1	-	-	0.1706	0.1772171
-	-	0.5	-	-	0.1747	0.1734302
-	-	1.0	-	-	1.777	0.1736992
-	-	-	0.2	-	0.1730	0.1753228
-	-	-	0.1	-	0.1684	0.1686163
-	-	-	-	0.5	0.1740	0.1792743
-	-	-	-	1.0	0.1754	0.1705923
-	-	-	-	1.5	0.1759	0.1710364

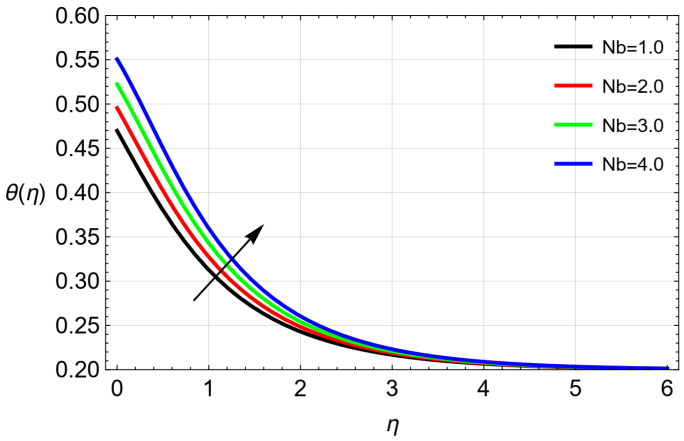

Figure 18. Plot the graph Brownian motion Nb on temperature.

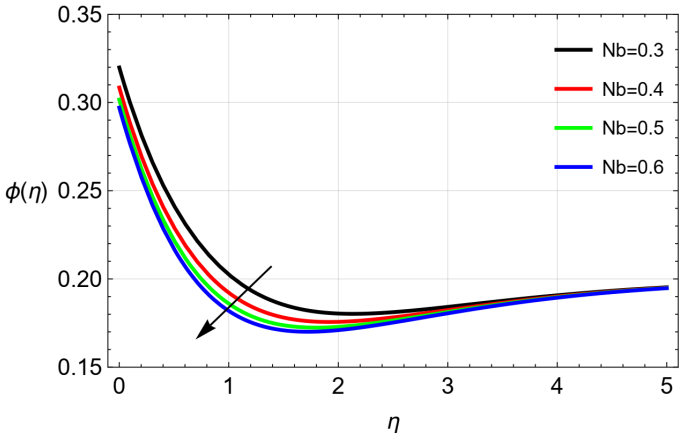

Figure 19. Plot the graph Brownian motion Nb on concentration.

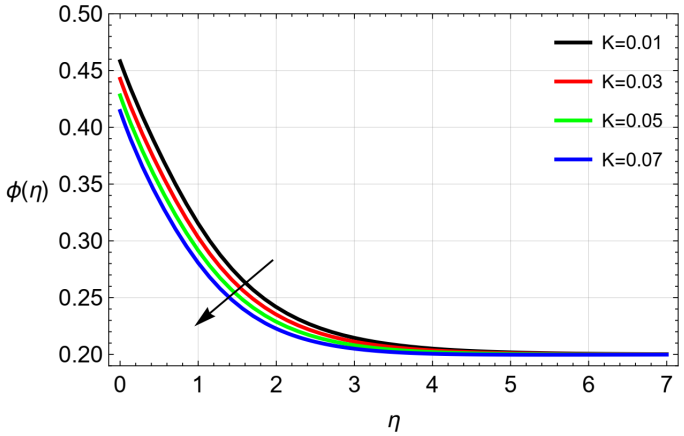

Figure 20. Plot the graph chemical reaction K on concentration.

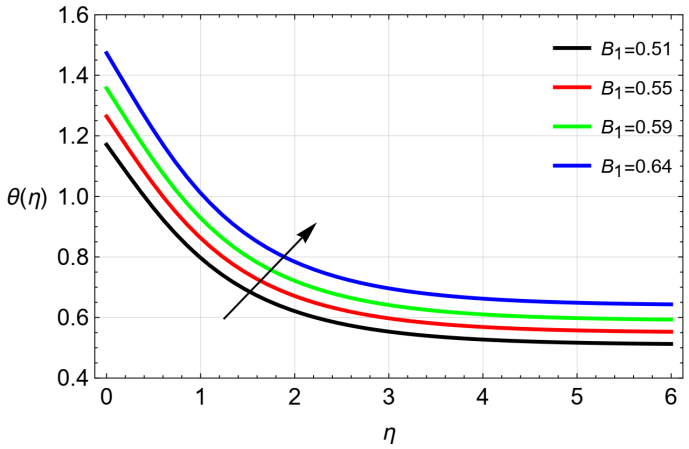

Figure 21. Plot the graph Biot number on temperature.

further increases the particle concentration in that area and even then, lessens the profile of the temperature. Knowing this, it is easy to understand the way the temperature differences affect particle distribution and thermal behavior. As shown in Figures 18 and 19,

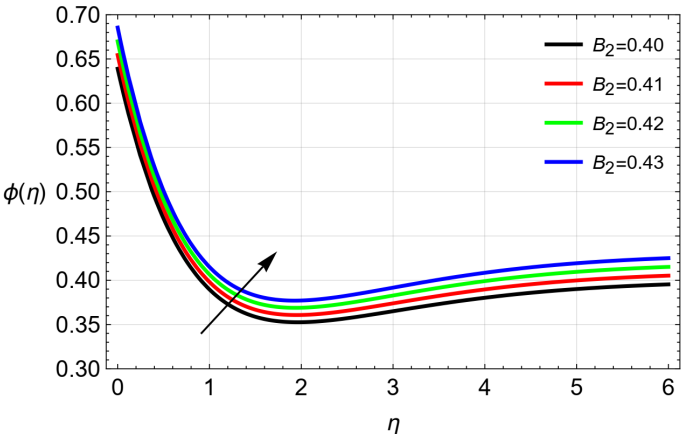

Figure 22. Plot the graph Biot number on concentration.

the Brownian motion parameter Nb enhances random movement of the particles to make them more equally distributed in the fluid. This diffusion minimizes the concentration of particles in nearby small regions. Brownian motion leads to greater random movement and causes a more equal distribution of particles and extends local concentrations. The effect that the chemical reaction parameter K has on temperature in Figure 20 differs in the sense that the reaction itself does not change temperature, but it aids in the dispersal of heat more uniformly across a system rather than concentrating specific regions to high temperatures. It also accelerates the rate of reaction with a subsequent increase in the concentration of product and a subsequent decrease in the concentration of a reactant. Figures 21 and 22 show that increasing Biot numbers (Bi_1, Bi_2) causes greater temperature differences within the object, inducing smaller rates of temperature change on the inside. They also develop a smaller scale concentration profile close to the surface in heat and mass transfer systems.

A numerical approach to the flow problem demands verifying the accuracy of the results as designated by these numbers. We provide a table of a comparison of our results with those of Nadeem et al. [37], Malik et al. [38], Bilal et al. [39], and Jakhar et al. [40], but focusing on values of $\frac{\sqrt{Re}C_f}{2}$ values of our problem. The quality of our scoring is well evidenced by our results, which fall in excellent accordance with those of previous studies. The validation technique serves to illustrate that our method of simulating the problem of the flow is reliable, and it has a different level of agreement with other studies. Table 1 compares values of $-\left(\frac{\lambda}{2}f''(0)^2 + f''(0)\right)$ with previously published work to validate the precision of the numerical approach used.

This section presents the numerical values of key physical characteristics—skin friction, Nusselt number, and Sherwood number—as listed in Tables 2–4, with selected flow parameters held constant. Table 2 shows that increasing the curvature parameter γ and magnetic field parameter M enhances skin friction through elevated shear stress, whereas a higher Weissenberg number λ reduces it by strengthening elastic effects that weaken velocity gradients; the Hall current parameter m has negligible impact. Tables 3 and 4 illustrate the sensitivity of the local Nusselt and Sherwood numbers to variations in thermal conductivity, radiation, Prandtl number, heat generation, Brownian motion, thermophoresis, Schmidt number, and chemical reaction. The Nusselt number rises with larger radiation parameter Rd, thermal conductivity parameter ϵ, Prandtl number Pr, and heat generation parameter β due to enhanced radiative and conductive heat transfer, but decreases with increasing thermophoresis Nt, Brownian motion Nb, and slightly with curvature parameter γ. The Sherwood number increases with higher thermophoresis Nt, chemical reaction parameter K, and Schmidt number Sc owing to strengthened mass diffusion and reaction rates, while it decreases with larger Brownian motion Nb and curvature parameter γ because of intensified particle dispersion. Overall, this analysis highlights how these parameters collectively govern fluid dynamics, heat, and mass transfer. Furthermore, Tables 1–4 confirm that the OHAM method achieves higher accuracy with fewer computations than BVP4C, exhibiting faster convergence and effective handling of nonlinear problems.

5 Conclusion

This paper focused on the flow of Williamson nanofluid on a stretched cylinder, taking into consideration the magnetic fields, the Hall current, chemical reaction, non-Fourier heat and mass transportation with the help of Cattaneo-Christov model. The gelling dynamics in the form of nonlinear governing equations were solved in an analytical mode wherein Optimal Homotopy Analysis Method (OHAM) yields viable and computationally flexible solutions.

- The parameter associated with the magnetic field M slowed down fluid velocity through the Lorentz resistance, and could be utilized in the flow control of the applications dealing with MHD;

- Hall parameter m changed the direction of a flow,

which means it enhanced radial velocity and, at the same time, decreased the axial one; it is significant in electromagnetic and plasma-based systems;

- Chemical reaction parameter (K) dimished nanoparticle concentration in the vicinity of the surface meaning that it is involved in the reactive transport processes such as drug delivery and catalysis;

- Thermal relaxation λ_t reduced heat transfer rate, and demonstrated the relevance of non-Fourier models in transient thermal systems where fluctuations play a prominent role in the mission;

- Higher thermophoresis parameter Nt increased the temperature profiles and thicker thermal layers, which enhanced the heat transport in nanofluid driven devices;

The advanced transport models coupled with the OHAM solution technique gave realistic results in non-Newtonian nanofluid behavior. The results may be used in the design of thermal engineering systems, materials processing systems and biomedical systems. Future work can involve time dependent flows, property dependence, experimental validation.

Data Availability Statement

Data will be made available on request.

Funding

This work was supported without any funding.

Conflicts of Interest

The authors declare no conflicts of interest.

Ethical Approval and Consent to Participate

Not applicable.

Nomenclature

u, w	Velocity components
(r, θ, z)	Cylindrical coordinate
B_o	Magnetic field strength
α	Variable caloric diffusivity
r	Radius of cylinder
D_B	Brownian motion coefficient
D_T	Thermophoretic coefficient
U_o	Reference velocity
R	Radius of cylinder
K_m	Mass exchange coefficient
h_T	Heat exchange coefficient
Q	Heat Source
q_r	Radiative heat flux
C_p	Specific heat
τ	Local skin friction
σ^*	Steffan–Boltzman constant
K^*	Mean absorption coefficients
T	Fluid temperature
T_w	Surface thermal
T_∞	Ambient temperature
C	Fluid concentration
C_w	Surface solutal
C_∞	Ambient Concentration
β	Heat generation
m	Hall parameter
M	Magnetic field
Pr	Prandtl number
Rd	Thermal radiation
Sc	Schmidt number
Nt	Thermophoresis parameter
Nb	Brownian motion
K	Chemical reaction parameter
λ_t	Thermal relaxation parameters
λ_c	Concentration relaxation parameters
Bi	Biot number
Re	Reynolds number
C_f	Skin friction
Nu	Nusselt number
Sh	Sherwood number
Symbols	
v	Kinematic viscosity
Γ	Williamson parameter
ρ	Density of fluid
$J \times B$	Lorentz force
ϵ_1	Heat relaxation time
ϵ_2	Mass relaxation time
Ψ	Stream function

η	Similarity variable
θ	dimensionless fluid temperature
ϕ	dimensionless fluid concentration
α_∞	Thermal conductivity
λ	Weissenberg number
σ	Electrical conductivity
γ	Curvature parameter
ϵ	Thermal conductivity parameter
Subscripts	
w	Evaluated at the wall/surface
∞	Ambient condition
0	Base state (e.g., μ_0 base viscosity)
Abbreviations	
MHD	Magnetohydrodynamic
OHAM	Optimal Homotopy Analysis Method
PDEs	Partial Differential Equations
ODEs	Ordinary Differential Equations
CCHF	Cattaneo Christov heat flux
CCMF	Cattaneo Christov mass flux

References

[1] Das, S. K., Choi, S. U., Yu, W., & Pradeep, T. (2007). *Nanofluids: science and technology*. John Wiley & Sons.

[2] Böhme, G. (2012). *Non-Newtonian fluid mechanics* (Vol. 31). Elsevier.

[3] Makkar, V., Poply, V., & Sharma, N. (2023). Three dimensional modelling of magnetohydrodynamic bio-convective Casson nanofluid flow with buoyancy effects over exponential stretching sheet along with heat source & gyrotactic micro-organisms. *Journal of Nanofluids, 12*(2), 535-547. [Crossref]

[4] Turkyilmazoglu, M., & Pop, I. (2024). Flow and heat transfer in annuli owing to inner shrinking and outer stationary cylinder. *Chinese Journal of Physics, 89*, 1899-1907. [Crossref]

[5] Hamid, A., Muhammad, T., & Irfan, M. (2024). Diffusions of nanoparticles and existence of multiple solutions for MHD Williamson nanofluid with slip mechanism. *Scientia Iranica*. [Crossref]

[6] Harfouf, A. E., Mounir, S. H., Mejdal, M., Mes-Adi, H., Herbazi, R., Rasool, G., ... & Nfaoui, M. (2024, October). Analysis of Magnetohydrodynamics Williamson Fluid's Thermal Radiation and Ohmic Heating Effects via an Inclined Channel. In *International Conference Interdisciplinarity in Engineering* (pp. 382-401). Cham: Springer Nature Switzerland. [Crossref]

[7] Khan, S. U., Riaz, A., & Ramesh, K. (2025). ACCELERATING BIOCONVECTIVE FLOW OF MICROPOLAR NANOFLUID DUE TO POROUS OSCILLATORY SURFACE WITH NONLINEAR THERMAL RADIATION, VISCOUS DISSIPATION AND SUCTION EFFECTS. *Journal of Porous Media, 28*. [Crossref]

[8] Ramzan, M., Bilal, M., & Chung, J. D. (2017). Radiative Williamson nanofluid flow over a convectively heated Riga plate with chemical reaction-A numerical approach. *Chinese Journal of Physics, 55*(4), 1663-1673. [CrossRef]

[9] Nadeem, S., Ishtiaq, B., Alzabut, J., & Ghazwani, H. A. (2024). Entropy generation for exact irreversibility analysis in the MHD channel flow of Williamson fluid with combined convective-radiative boundary conditions. *Heliyon, 10*(4). [Crossref]

[10] Ahmad, S., Ahammad, N. A., Khan, M. N., Algehyne, E. A., Tag-Eldin, E., Gepreel, K. A., ... & Galal, A. M. (2022). Thermal and solutal energy transport analysis in entropy generation of hybrid nanofluid flow over a vertically rotating cylinder. *Frontiers in Physics, 10*, 988407. [Crossref]

[11] Turkyilmazoglu, M. (2021). Exact solutions concerning momentum and thermal fields induced by a long circular cylinder. *The European Physical Journal Plus, 136*(5), 1-10. [Crossref]

[12] Shah, Z., Alzahrani, E. O., Alghamdi, W., & Ullah, M. Z. (2020). Influences of electrical MHD and Hall current on squeezing nanofluid flow inside rotating porous plates with viscous and joule dissipation effects. *Journal of Thermal Analysis and Calorimetry, 140*(3), 1215-1227. [Crossref]

[13] Turkyilmazoglu, M. (2024). Evidence of stretching/moving sheet-triggered nonlinear similarity flows: atomization and electrospinning with/without air resistance. *International Journal of Numerical Methods for Heat & Fluid Flow, 34*(9), 3598-3614. [Crossref]

[14] Cattaneo, C. (1948). Sulla conduzione del calore. *Atti Sem. Mat. Fis. Univ. Modena, 3*, 83-101. [Crossref]

[15] Ván, P., & Fülöp, T. (2012). Universality in heat conduction theory: weakly nonlocal thermodynamics. *Annalen der Physik, 524*(8), 470-478. [Crossref]

[16] Ali, A., Khatoon, R., Ashraf, M., & Awais, M. (2022). Cattaneo–Christov heat flux on MHD flow of hybrid nanofluid across stretched cylinder with radiations and Joule heating effects. *Waves in Random and Complex Media*, 1-18. [Crossref]

[17] Khan, M., Shahid, A., Salahuddin, T., Malik, M. Y., & Hussain, A. (2020). Analysis of two dimensional Carreau fluid flow due to normal surface condition: A generalized Fourier's and Fick's laws. *Physica A: Statistical Mechanics and its Applications, 540*, 123024. [Crossref]

[18] Sohail, M., & Nazir, U. (2023). Numerical computation of thermal and mass transportation in Williamson material utilizing modified fluxes via optimal homotopy analysis procedure. *Waves in Random and Complex Media*, 1-22. [Crossref]

[19] Nadeem, S., Ahmad, S., & Muhammad, N. (2017). Cattaneo-Christov flux in the flow of a viscoelastic fluid in the presence of Newtonian heating. *Journal of*

Molecular liquids, 237, 180-184. [Crossref]

[20] Li, X., Abbasi, A., Al-Khaled, K., Ameen, H. F. M., Khan, S. U., Khan, M. I., ... & Guedri, K. (2023). Thermal performance of iron oxide and copper (Fe3O4, Cu) in hybrid nanofluid flow of Casson material with Hall current via complex wavy channel. *Materials Science and Engineering: B, 289*, 116250. [Crossref]

[21] Shafiq, A., Khan, I., Rasool, G., Seikh, A. H., & Sherif, E. S. M. (2019). Significance of double stratification in stagnation point flow of third-grade fluid towards a radiative stretching cylinder. *Mathematics, 7*(11), 1103. [Crossref]

[22] Khan, M. N., Alhuthali, A. M., Amjad, A., Saqlain, M., Yar, M., Alshammry, N., & Elkotb, M. A. (2024). Numerical investigation of mixed convective flow of micropolar Casson fluid with Cattaneo–Christov heat flux model on an inclined vertical stretching surface. *Journal of Computational Design and Engineering, 11*(3), 174-184. [Crossref]

[23] Ali, F., Padmavathi, T., & Hemalatha, B. (2025). Entropy minimization in Darcy Forchheimer on Sutterby nanofluid past a stretching surface with swimming of gyrotactic microorganisms. *Waves in Random and Complex Media, 35*(5), 10333-10356. [CrossRef]

[24] Khan, N. S., Gul, T., Islam, S., Khan, A., & Shah, Z. (2017). Brownian motion and thermophoresis effects on MHD mixed convective thin film second-grade nanofluid flow with Hall effect and heat transfer past a stretching sheet. *Journal of Nanofluids, 6*(5), 812-829. [Crossref]

[25] Sohail, M., Rafique, E., & Abodayeh, K. (2024). Boundary layer analysis on magnetohydrodynamic dissipative Williamson nanofluid past over an exponentially stretched porous sheet by engaging OHAM. *Multidiscipline Modeling in Materials and Structures, 20*(6), 973-994. [Crossref]

[26] Hussain Shah, S. Z., Ayub, A., Khan, U., Darvesh, A., Sherif, E. S. M., & Pop, I. (2024). Thermal transport exploration of ternary hybrid nanofluid flow in a non-Newtonian model with homogeneous-heterogeneous chemical reactions induced by vertical cylinder. *Advances in mechanical engineering, 16*(5), 16878132241252229. [Crossref]

[27] Abbas, Z., Naveed, M., & Sajid, M. (2013). Heat transfer analysis for stretching flow over a curved surface with magnetic field. *Journal of Engineering Thermophysics, 22*(4), 337-345. [CrossRef]

[28] Zaman, S. U., Aslam, M. N., Riaz, M. B., Akgul, A., & Hussan, A. (2024). Williamson MHD nanofluid flow with radiation effects through slender cylinder. *Results in Engineering, 22*, 101966. [Crossref]

[29] Rauf, A., Faisal, Shah, N. A., & Botmart, T. (2022). Hall current and morphological effects on MHD micropolar non-Newtonian tri-hybrid nanofluid flow between two parallel surfaces. *Scientific Reports, 12*(1), 16608. [Crossref]

[30] Rasheed, H. U., Khan, Z., El-Zahar, E. R., Shah, N. A., Islam, S., & Abbas, T. (2025). Homotopic solutions of an unsteady magnetohydrodynamic flow of Casson nanofluid flow by a vertical cylinder with Brownian and viscous dissipation effects. *Waves in Random and Complex Media, 35*(5), 9457-9470. [Crossref]

[31] Krishna, M. V., Bharathi, K., & Chamkha, A. J. (2018). Hall effects on MHD peristaltic flow of Jeffrey fluid through porous medium in a vertical stratum. *Interfacial Phenomena and Heat Transfer, 6*(3). [Crossref]

[32] Elsaid, E. M., Abd El-Aziz, M., Aly, A. M., Alruwaili, A. S., & Eid, M. R. (2024). Physical analysis and thermal case of magnetized fluid flow and heat transfer via stretchable cylinder: Hall impact and entropy generation. *Modern Physics Letters B, 38*(36), 2450371. [Crossref]

[33] Gul, T., Khan, A. S., Islam, S., Alqahtani, A. M., Khan, I., Alshomrani, A. S., ... & Muradullah. (2017). Heat transfer investigation of the unsteady thin film flow of Williamson fluid past an inclined and oscillating moving plate. *Applied Sciences, 7*(4), 369. [Crossref]

[34] Khan, W., Gul, T., Idrees, M., Islam, S., Khan, I., & Dennis, L. C. C. (2016). Thin film Williamson nanofluid flow with varying viscosity and thermal conductivity on a time-dependent stretching sheet. *Applied Sciences, 6*(11), 334. [Crossref]

[35] Awwad, F. A., Ismail, E. A., Khan, W., Gul, T., & Khan, A. S. (2023). Comparative numerical analysis for the error estimation of the fluid flow over an inclined axisymmetric cylinder with a gyrotactic microbe. *Symmetry, 15*(10), 1811. [Crossref]

[36] Gul, T., & Afridi, S. (2018). The heat and mass transfer analysis during bunch coating of a stretching cylinder by Casson fluid. In *Fluid Flow Problems*. IntechOpen. [Crossref]

[37] Nadeem, S., Hussain, S. T., & Lee, C. (2013). Flow of a Williamson fluid over a stretching sheet. *Brazilian journal of chemical engineering, 30*, 619-625. [Crossref]

[38] Malik, M. Y., Bibi, M., Khan, F., & Salahuddin, T. (2016). Numerical solution of Williamson fluid flow past a stretching cylinder and heat transfer with variable thermal conductivity and heat generation/absorption. *AIP Advances, 6*(3). [Crossref]

[39] Bilal, M., Sagheer, M., & Hussain, S. (2018). Numerical study of magnetohydrodynamics and thermal radiation on Williamson nanofluid flow over a stretching cylinder with variable thermal conductivity. *Alexandria engineering journal, 57*(4), 3281-3289. [Crossref]

[40] Jakhar, A., Sukariya, V. K., Kumar, S., Kumar, A., & Anurag. (2024). Study of MHD Williamson fluid flow over a stretched cylinder with Hall, thermal dynamics, and chemical reactions effects. *Journal of Thermal Analysis and Calorimetry*, 1-18. [Crossref]

[41] Sohail, M., Rafique, E., Mahariq, I., & Qureshi, I. H. (2024). Analytical investigation via OHAM on thermally magnetized non-Newtonian Williamson fluid with heat generation and thermal radiation effects. *Proceedings of the Institution of Mechanical Engineers, Part N: Journal of Nanomaterials, Nanoengineering and Nanosystems*, 23977914251338150. [Crossref]

[42] Omar, H. A. (2021). An integrated genetic algorithm and homotopy analysis method to solve nonlinear equation systems. *Mathematical Problems in Engineering, 2021*(1), 5589322. [Crossref]

[43] Pathak, S., & Singh, T. (2015). Optimal homotopy analysis methods for solving the linear and nonlinear fokker-planck equations. *British Journal of Mathematics & Computer Science, SCIENCEDOMAIN international, 7*(3), 209-217.

[44] Jasim, M., Anakira, N., Kamel, L., Amourah, A., Fareed, A., & Al Kalbani, K. S. (2024). Improved solutions of oham approximate procedure for classes of nonlinear odes. *Contemporary Mathematics, 5*(3), 4115. [Crossref]

[45] Anakira, N. R., Alomari, A. K., Jameel, A. F., & Hashim, I. (2017). Multistage optimal homotopy asymptotic method for solving boundary value problems with robin boundary conditions. *Far East Journal of Mathematical Sciences, 102*(8), 1727-1744. [Crossref]

[46] Bahia, G., Ouannas, A., Batiha, I. M., & Odibat, Z. (2021). The optimal homotopy analysis method applied on nonlinear time-fractional hyperbolic partial differential equation s. *Numerical Methods for Partial Differential Equations, 37*(3), 2008-2022. [Crossref]

Nimra Riaz has completed MS Mathematics from Khwaja Fareed University of Engineering and Information Technology Rahim Yar Khan, Pakistan and her interest is in fluid mechanics. (Email: math231501014@kfueit.edu.pk)

Muhammad Sohail belongs to a very small village of district Haripur, Khyber Pakhtunkhwa, Pakistan. He got his PhD Mathematics degree from the Institute of Space Technology Islamabad, Pakistan in 2020. Currently, he is working as an Assistant Professor Mathematics at Khwaja Fareed University of Engineering and Information Technology Rahim Yar Khan, Pakistan. His research interests are on CFD simulation, mass transport, heat transfer, mathematical modelling, nonlinear dynamics, stability analysis, numerical and analytical methods, fractional differential equations, mixed convection and heat exchangers. He has published more than about 200 research articles in different peer reviewed international journals. (Email: muhammad.sohail@kfueit.edu.pk ; muhammad_sohail111@yahoo.com)